

## TE Field Integration for Electromagnetic Sensors

Ian Woodhead, Ian Platt  
Lincoln Technology  
Lincoln Ventures Ltd, Lincoln University, Canterbury, New Zealand  
woodhead@lincoln.ac.nz

### Abstract

The use of time domain reflectometry (TDR) techniques for measuring the moisture content of composite materials is a mature art but usually assumes homogeneity of the material in the transverse plane. As the basis of a forward solution to TDR imaging, we describe an integral equation approach to model the response of the TDR system to a lossless heterogeneous dielectric body. Then, in conjunction with a suitable dielectric model of the composite material, the TDR response to moisture content distribution may be quantified.

Several methods for integrating the transverse electromagnetic field between the transmission line rods were compared and a method combining *a priori* information with linear interpolation provided the most consistent integration for three different permittivity distributions. A self-consistency approach was used to compare the modelled propagation velocity with that expected from transmission line theory.

**Keywords:** TDR, heterogeneous, dielectric, imaging, interpolation.

### 1 Introduction

Time domain reflectometry (TDR) is used extensively for measurement of  $\theta$ , the volumetric moisture content in soil, and is applicable but less widely used in other materials such as grains, powders, and minerals. An open-ended transmission line, typically 300 mm long, is buried in the material under test. The travel time of a pulse with typical risetime of 300 ps provides the mean propagation velocity  $v$ , on the line of known length. Since most biological and composite materials do not contribute to the permeability of the region,  $v$  indicates the mean relative permittivity  $\epsilon_r$  of the material surrounding the transmission line. When the loss tangent is small and the relative permeability is one,  $\epsilon_r \approx \frac{c^2}{v^2}$ , where  $c$  is the velocity of light. Since  $\epsilon_r$  for most dry organic and composite materials is in the range of 3 to 5 whereas that of water is typically 80, the measured  $\epsilon_r$  provides a useful indication of its moisture content. Empirical calibration techniques are normally used. Topp *et al* [1] for example, used measurements on a range of soils, to develop a polynomial relating the measured  $\epsilon_r$  to  $\theta$ . This particular calibration is applicable to quite a wide range of soil types (and hence orders of magnitude variation in particle size with their attendant variable interactions with water molecules) and typically has an accuracy of better than 2% in  $\theta$  over the range 5 to 50%.

In those situations where it is not desirable to bury the transmission line sensor into the material, non-invasive techniques may be employed. Dielectric measurements in the microwave range may use a signal launched into the material from a horn or planar antenna, or use the evanescent field of a parallel transmission line. Examples of the former have been used for medical imaging [2] and land-mine detection [3]. The use of an evanescent field circumvents reflection and diffraction effects and has been used for measurement of surface soil moisture [4] and other materials [5], but apparently not for quantifying permittivity and other [5] distributions.

We utilise the lateral, evanescent field of a parallel transmission line to shallowly probe the interior of a composite material and hence determine the moisture content distribution. The process involves two distinct steps. The first is the forward problem defined for this work as predicting  $v$  on a parallel transmission line given a known permittivity distribution surrounding the line [6]. The second step is the inverse problem. It reconstructs the permittivity and hence moisture content distribution given a set of measurements of  $v$  for different physical positions of the parallel transmission line in relation to the permittivity distribution [7].

An integral equation (IE) method has been chosen as the forward model for use with our tomographic inversion algorithms, and exploits two important characteristics of IE methods. The first is that where the region of anomalous permittivity is surrounded by free space, only the anomalous region needs to be calculated. The second advantage of an IE approach relates directly to tomography, since several different distributions of impressed field are required to provide additional information, to distinguish the moisture content of different zones. When changing the impressed electric field, matrix recalculation is unnecessary. However, a disadvantage of IE methods is that when applied to arbitrary permittivity distributions, volume integration is required even when one dimension is invariant. Under these circumstances as in the present case, quasi 3-D or 2.5-D variants reduce the computational burden of the IE method to compare more favourably with the differential equation approach.

We first briefly describe the formulation of the IE solution assuming a lossless inhomogeneous medium surrounding a parallel transmission line, and the method for constructing the impressed field distribution of the line. Several methods of integrating the field between the lines to enhance accuracy will then be shown, including our approach that combines *a priori* information with linear interpolation. Finally, validation using self-consistency and comparison with measured values is presented.

## 2 Integral Equation

The polarisation of a discretised zone or cell within a dielectric material may be represented by a dipole at its geometric centre. In most dielectric materials, there is no net polarisation until generated by an external or impressed field. When applied to this quasi-static electric field problem, the method of moments may be considered as the summation in each cell, of the electric field contributions due to the polarisation in all other cells. The potential  $\phi_p$  at point  $p(x,y,z)$  generated by a dipole with dipole moment or polarisation  $\mathbf{P}$ , is:

$$\phi_p = \frac{\mathbf{P} \cdot \hat{\mathbf{r}}}{4\pi\epsilon_0 r^2} \quad (1)$$

where  $\hat{\mathbf{r}}$  is a unit vector pointing from the centre of the dipole to  $p$  [8]. Its electric field is the space rate of change of potential ( $-\nabla\phi_p$ ) so that for Cartesian coordinates,  $\nabla\phi = \hat{\mathbf{x}}\phi_x + \hat{\mathbf{y}}\phi_y + \hat{\mathbf{z}}\phi_z$ . Then since  $\frac{dr}{dx} = \frac{x}{r}$  and  $\mathbf{x} = x\hat{\mathbf{x}}$ ,

$$E_{px} = \frac{-\mathbf{P}}{4\pi\epsilon_0 r^5} \left[ \hat{\mathbf{x}}(r^2 - 3x^2) - \hat{\mathbf{y}}(3xy) - \hat{\mathbf{z}}(3xz) \right] \quad (2)$$

and with corresponding equations for  $E_{py}$  and  $E_{pz}$ , may be expressed as a dyadic equation

$$\mathbf{E}_p = \frac{\mathbf{P}}{4\pi\epsilon_0 r^5} \begin{bmatrix} \hat{\mathbf{x}}\hat{\mathbf{x}}(3x^2 - r^2) + \hat{\mathbf{x}}\hat{\mathbf{y}}(3xy) + \hat{\mathbf{x}}\hat{\mathbf{z}}(3xz) \\ \hat{\mathbf{y}}\hat{\mathbf{y}}(3y^2 - r^2) + \hat{\mathbf{y}}\hat{\mathbf{x}}(3xy) + \hat{\mathbf{y}}\hat{\mathbf{z}}(3yz) \\ \hat{\mathbf{z}}\hat{\mathbf{z}}(3z^2 - r^2) + \hat{\mathbf{z}}\hat{\mathbf{x}}(3zx) + \hat{\mathbf{z}}\hat{\mathbf{y}}(3zy) \end{bmatrix} \quad (3)$$

We may combine the above in an integral equation describing the electric field  $\mathbf{E}_p$  at a point  $p$ :

$$\mathbf{E}_p(x,y,z) = -\nabla \left( \iiint \frac{\mathbf{P} \cdot \hat{\mathbf{r}}}{4\pi\epsilon_0 r^2} dv \right) \quad (4)$$

where  $dv$  is the differential volume over which each  $\mathbf{P} \cdot \hat{\mathbf{r}}$  applies. The polarisation region may be discretised, and following the method of moments [9], we calculate the matrix of polarisation vectors  $\mathbf{P}(x,y,z)$  using

$$L(\mathbf{P}) = -\mathbf{E}_i(x,y,z) = \mathbf{E}_p(x,y,z) - \frac{\mathbf{P}(x,y,z)}{\epsilon_0\chi(x,y,z)} \quad (5)$$

where  $L$  is a linear operator,  $\mathbf{E}_i$  the external impressed field and  $\chi(x,y,z)$  the susceptibility ( $\epsilon_r(x,y,z) - 1$ ). Equation 8 is converted to matrix form and solved for the vector of polarisations  $\mathbf{P}$ , and the electric field strength in each cell is recovered from the polarisation:

$$\mathbf{E}(x,y,z) = \frac{\mathbf{P}(x,y,z)}{\epsilon_0\chi(x,y,z)} \quad (6)$$

The inputs required for the method are: a vector comprising sets of three elements describing the impressed field, a matrix describing the permittivity within each cell, and the dimensionality of the problem. While the above method applies to any impressed field distribution, in this case  $\mathbf{E}_i$  is the vector of impressed field components due to a parallel transmission line. To obtain the potential difference between the two lines and hence determine line capacitance, the field described by matrix  $\mathbf{E}$  is integrated along a path connecting the two transmission line rods (along the x-axis for example). Then to obtain the velocity of an electrical edge on the transmission line (assumed lossless), the standard transmission line formula is used:

$$v = \frac{1}{\sqrt{LC}} = \sqrt{\frac{\pi \int \mathbf{E}(x,y,z) \cdot d\mathbf{l}}{q\mu \cosh^{-1}\left(\frac{b}{a}\right)}} \quad (7)$$

Here  $dl$  is the length element of the numerical integration (the cell length in this discretised case),  $q$  the same initial line charge density that defined the impressed field,  $\mu$  the total permeability,  $b$  the transmission line rod spacing, and  $a$  the rod diameter.

### 3 Integration of the Electric Field

The result of the moment method calculation is a map of the electric field strength in each cell of the discretised zone. In this case,  $E_i$  is configured to represent the free space TE field for a parallel transmission line using electrostatic techniques. To then calculate the capacitance per unit length of transmission line and thereby enable calculation of the propagation velocity, a line integral of the field between the transmission line rods is performed.

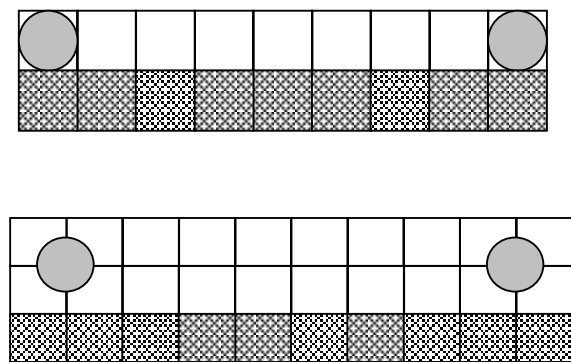


**Figure 1.** Alignment of transmission line rods at (a) cell centre, (b) cell intersections.

The field generated by the transmission line rods is little different from that of a line charge, and the line may be chosen to be at the centre of a cell (Fig. 1a), or at the intersection of cells (Fig. 1b). Both methods have been used and provided accurate results. In the former case the cell size may be conveniently chosen to match the size of the transmission line rods thereby assisting integration of the field. This also allows the anomalous region, that is with non zero susceptibility, to be very close to the rods (hatched cells in figure 1a). However, an advantage of positioning the transmission line rods at cell intersections is that self consistency may be used to test the accuracy of the solution as described below. A further advantage of locating the centre of the rods at cell boundaries is that the singularities that occur at the centre of the line charge are relegated to cell boundaries, not the cell mid points where the fields are calculated. Thus, the line integration may usefully integrate just between cell centres. When the rods are coincident with the cells, extrapolation may be used to integrate out to the cell boundaries that coincide with the rod boundaries.

Various techniques for integrating the electric field to obtain the potential difference between the transmission line rods will now be presented.

#### 3.1 Coarse Integration

Coarse integration simply comprises a numerical line integral using the field points calculated from the forward model so that

$$V = \sum_{rod1}^{rod2} E_i \Delta x_i \quad (9)$$

While the accuracy of integration may be easily improved by finer discretisation and hence smaller  $\Delta x_i$ , extending the size of the forward model by finer discretisation greatly increases memory use and execution time. Further, since this work is being applied to measurement of travel time on a parallel transmission line, it requires a timing instrument with very high resolution to finely resolve the influence of discretised regions near the line. Hence, finer discretisation puts greater demands on the instrumentation required to solve the TDR imaging problem, so means of interpolating the discretised cells were sought with the aim of producing more accurate integration of the field. Note that to better represent the transmission line rods by cells of square cross section would require the rod diameter to be represented by three cells, greatly increasing the size of the problem.

#### 3.2 Linear Interpolation

All methods of improving the accuracy of the numerical integration involve an interpolation technique whereby an inference is made about the nature of the field distribution between the (assumed accurate) electric field at the cell mid points. The most trivial is that of linear interpolation, which may be easily shown to be equivalent to coarse integration.

#### 3.3 Polynomial Interpolation

One approach to improving field integration is to fit a polynomial to the field data from the each cell, and integrate the fitted curve as representing a continuous function of field strength. As expected, polynomial curve fitting which requires continuous first derivatives, produced overshoot near step changes in permittivity. These were exacerbated as the order of the polynomial was increased to better match the high rate of change in field strength, and hence improve the accuracy of the line integrals. We therefore consider that polynomials are appropriate for field interpolation with inhomogenous dielectric materials.

A common approach to circumventing the interpolation difficulties inherent with the polynomial fitting where there are discontinuities or high rates of curvature in the data, is the use of splines. For example, the commonly used cubic polynomial may be fitted between adjacent data points to produce a curve through all the data points. If one spline fit is used, both first and second derivatives are continuous. Conversely, if cubic splines are separately applied to each side of a discontinuity, discontinuous derivatives result, but the method requires careful analysis of the data to locate such discontinuities.

### 3.4 Characteristic Interpolation

An approach that we currently favour and that is believed to be new at least to this application incorporates *a priori* knowledge of the nature of the curve. This method uses existing knowledge of the nature of the field distribution near a parallel transmission line to interpolate between the cells. As shown earlier for a rectangular grid in a Cartesian plane, the  $x$  component of the field is:

$$E_x = \frac{1}{2\pi\epsilon_0} \left( \frac{-q(x + \frac{b}{2})}{(x + \frac{b}{2})^2 + y^2} + \frac{q(\frac{b}{2} - x)}{(\frac{b}{2} - x)^2 + y^2} \right) \quad (8)$$

For a homogenous permittivity and the transmission line rods centred on the  $x$ -axis (hence  $E_y = 0$ ), with

$y = 0$ , and for convenience the transmission line is shifted by  $x = b/2$ :

$$E_x = \frac{-q}{2\pi\epsilon_0\epsilon_r} \left( \frac{1}{x} + \frac{1}{b-x} \right) \quad (9)$$

Then given a known  $E_x$ , an effective relative permittivity  $\epsilon_r$  may be calculated to describe the field near the known value. In practice it is convenient to incorporate all the constants into one value  $k$ , so that:

$$k = \frac{E_x}{\left( \frac{1}{x} + \frac{1}{b-x} \right)} \quad (10)$$

Initially, the method was evaluated by comparing a numerical method of calculating the capacitance of a parallel transmission line in a homogenous dielectric with the known analytical form. The above procedure was implemented using a transmission line rod spacing  $b$  of 0.1 m, diameter  $a$  of 0.005 m, and a relative permittivity  $\epsilon_r$  of 1. Twenty cells of dimension 0.005 m were used for the numerical calculation using the moment method, with characteristic interpolation providing 10 subsamples within each cell. The numerical approach integrated the field between the cells using arbitrary  $q$  to obtain

the voltage, and thereby determine the line capacitance. The analytic form for the capacitance of a parallel transmission line provided an exact solution [10]:

$$C = \frac{\pi\epsilon_0\epsilon_r}{\cosh^{-1}\left(\frac{b}{a}\right)} \quad (11)$$

The calculated capacitance using a 20 cell numeric method changed from 8.36 pF/m to 7.58 pF/m when incorporating the subsampling, whereas the analytic solution was 7.538 pF/m. While providing the expected enhanced accuracy in the above case, characteristic interpolation was less useful with an inhomogenous permittivity since differing values of the constant  $k$  in adjacent cells resulted in incorrect curvature and a discontinuity in the field strength at the cell boundaries. Instead, the value of  $k$  was linearly interpolated between cell midpoints to provide a continuous field strength function, although the first derivative was still discontinuous. Fig. 6 demonstrates the improvement. Polynomial interpolation of  $k$  resulted in deviations from the expected field distribution, as discussed below.

### 3.5 Extrapolation

Extrapolation is necessary to integrate that portion of the field between the surface or edge of the transmission line rod (in the case of figure 1a), and the centre of the adjacent cell. The field near the rod rapidly rises in strength, and while extrapolation using linear techniques is relatively safe but inaccurate, extrapolation when using a polynomial fit is known to be unsatisfactory. Outside the domain of the data, the polynomial usually diverges sharply from that which may be expected from visualising the data (figure 4 spline curve), particularly when higher order polynomials are used.

The characteristic method provides extrapolation that follows the theoretical shape of the field strength to the centre of the transmission line rod. Except for the negligible proximity effect, the presence of the rod introduces a limit on the magnitude of the field strength without altering the shape up to the edge of the rod. Hence whether the model represents the transmission line by a cell (as in figure 1a) or by a line charge (as in figure 1b) with infinite potential, the characteristic method is appropriate for extrapolating the field strength.

## 4 VALIDATION

Validation of the numerical model may be accomplished by comparison of the model output with measured propagation times or through self-

consistency [11]. The former method was described separately [6], and the latter approach will be described here. As described by [11], there is no energy exchange between the two half spaces intersecting an axis through the centres of the rods of a parallel transmission line. Hence, provided the permittivity in each half space is homogenous, the equivalent permittivity of the parallel transmission line is the arithmetic average of the half plane values. We chose to use similar values as in [11], comparing the results with half plane permittivities of 5 and 15, with those of 10 and 10. The method used a pseudo 3-D moment method that exploits the axial averaging characteristics of TDR in practical measurement situations [7] by including the influence of cells in the  $z$  direction within the 2-D ( $xy$ ) matrix. Thus integration of the axial field components during each calculation step in a chosen transverse plane, effectively reduces the 3-D volume integral equation method to 2-D.

Using a transverse plane of 20 by 20 cells, with a rod spacing of eight cells and a rod size of one cell, provided a good compromise between the size of the model (total number of cells), rod size and spacing, and the distance from a rod to the boundary of the modelled region. The model provides a direct prediction of propagation velocity ( $v_p$ ) from the permittivity distribution, which for the lossless case is  $v = \frac{c}{\sqrt{\epsilon_r}}$ . Table 1 shows the results from the

verification, which gave a 0.55% error in propagation velocity between the two permittivity distributions. The absolute error between the expected  $\frac{c}{\sqrt{10}}$  m/s and

calculated propagation velocities was larger, being influenced by the accuracy of integrating the field between the transmission line rods.

Table 1. Self-consistency of forward model.

$\epsilon_r$ in half space 1	$\epsilon_r$ in half space 2	Expected $v_p$ (m/s)	Modelled $v_p$ (m/s)
10-j0	10-j0	0.9487 x10 <sup>8</sup>	0.9563 x10 <sup>8</sup>
5-j0	15-j0	0.9487 x10 <sup>8</sup>	0.9616 x10 <sup>8</sup>

Integration of the electric field was validated using comparison of the model output with measured propagation times from a Tektronix 1502C connected with 0.8 m of URM 43 coaxial cable to a 1:4 balun and then to the parallel transmission line rods. Balun construction followed [13], but omitted the initial 1:1 transformer, and used a single, grade S3 ferrite toroid. A relay (similar to Teledyne 172) switched the balanced line to either a reference transmission line or the measuring line. The 6 mm diameter stainless steel

rods were spaced 60 mm apart, with the measuring rods 300 mm longer than the reference rods. At the end of the transmission lines 6 by 1mm steel shorting straps provided sharper, better defined reflections than unterminated lines. Waveform data retrieved from the 1502 were smoothed and differentiated using 25 point routines [14]. The intersection between the tangents to the maximum negative slope and the immediately preceding stationary point defined the edge of the pulse. Finally, the reading from the reference line was subtracted from that of the measuring line to obtain the actual travel time of the edge.

The results from the model with different integration methods and the measured values are given in Table 2 and represent the one-way travel time along the 300 mm transmission line rods. The conditions include no nearby dielectric material (air), a nearby phantom (asymmetric), and a binary distribution where one rod was immersed in water and the other in air. A rectangular thin walled plastic container 150 by 500 by 80 mm filled with water was used for the asymmetric distribution and the geometric centre of transmission line was positioned 8 mm above the top corner of the container (Fig. 4).

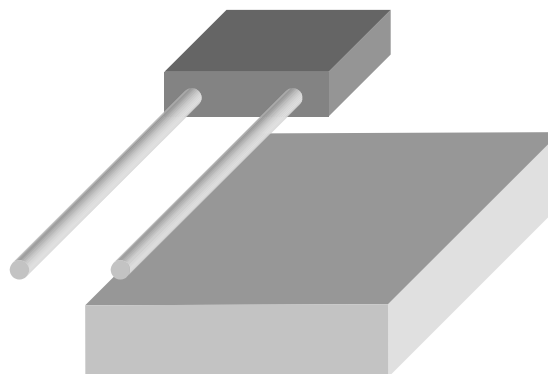


Figure 4. Arrangement of asymmetric permittivity distribution.

The data in the asymmetric and binary cases were corrected by subtracting the offset or time by which the air reading differed from 1.0 ns. No measurement has been made of the travel time in a binary distribution, which was included to highlight the differences with permittivity distributions that were more extreme than those expected when externally probing a dielectric material. Although the better extrapolation performance of the characterisation methods is apparent from the air readings, there was no significant difference between the methods after the offset correction had been subtracted.

**Table 2.** Propagation time (ns) comparisons of integration methods.

	Air (ns)	Asymmetric (ns) (corrected)	Binary (ns) (corrected)
Linear	1.042	1.040	1.450
Spline	1.024	1.036	1.526
Characteristic	1.004	1.037	1.436
Hybrid linear	1.003	1.037	1.414
Hybrid poly.	1.004	1.037	1.426
Measured	0.987	1.039	-

The difference in extrapolation is apparent from the anomalous electric field distribution in Fig. 5 where the spline method under-estimates the rapidly increasing field strength near the transmission line rods. The step changes of the non-interpolated characteristic method are also apparent. Fig. 6, although unrealistic for the probing application described here, indicates the expected poor extrapolation of the spline method and the larger steps in the non-interpolated characteristic method. However, what is more notable is oscillation of the polynomial-interpolated characteristic method (hybrid polynomial), which adds deviations from the expected shape of the field strength distribution in the region between 3 and 5.5 cm. In this case, the linearly interpolated (hybrid linear) curve provides the best fit and is well behaved near the transmission line rods.

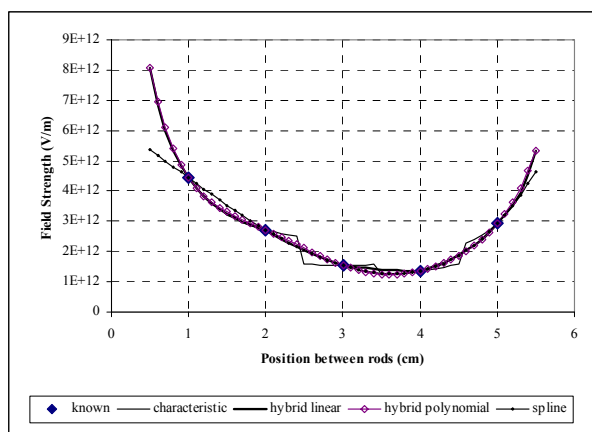


**Figure 5.** Field interpolation with asymmetric permittivity distribution.

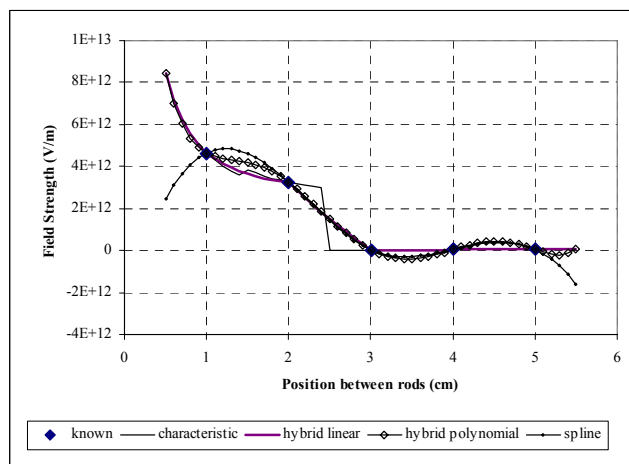


**Fig. 6.** Field interpolation with binary permittivity distribution.

## 5 Conclusions

A moment method solution has been described that determines the electric field distribution in a low loss, inhomogeneous dielectric material given a pre-determined impressed field  $E_i$ , which was derived for a parallel transmission line. Several methods for interpolating the field between calculated values were compared, and the best method combined information from the known field calculation for a parallel transmission line in a uniform permittivity with linear interpolation of permittivity between cells. The forward model was validated by comparing the predicted propagation velocity in a uniform permittivity with that from an equivalent binary permittivity distribution, and provided agreement within 0.6%. Incorporating the calculated capacitance of the parallel transmission line into the telegraphers equations to calculate the propagation velocity has enabled prediction of the impact of arbitrary dielectric (or moisture content) distributions on a TDR measurement system. It will also form the forward solution to a TDR imaging method for non-invasive determination of moisture distribution in composite materials.

## 6 Acknowledgements

The author's acknowledge support for this research from the New Zealand Foundation for Research Science and technology.

## 7 References

- [1] G. C. Topp, J. L. Davis, and A. P. Annan, "Electromagnetic Determination of Soil Water Content: Measurements in Coaxial Transmission Lines," *Water Resour. Res.*, Vol. 16, 1980, pp. 574-582.
- [2] Franchois and C. Pichot, "Microwave Imaging-Complex Permittivity Reconstruction with a Levenberg-Marquardt Method," *IEEE Transactions on Antennas and Propagation*, Vol. AP-45, 1997, pp. 203-215.
- [3] S. A Johnson, pers. comm., TechniScan Inc., Salt Lake City, Utah, 1999.
- [4] J. S. Selker, L. Graff, and T. Steenhuis, "Noninvasive Time Domain Reflectometry Moisture Measurement Probe," *Soil Sci. Soc. Am. J.*, Vol. 57, 1993, pp. 934-936.
- [5] S. S. Stuchly and C. E. Bassey, "Coplanar Microwave Sensor for Industrial Measurements," *12<sup>th</sup> Int. Conf. On Microwaves and Radar*, Vol. 3, 1998, pp. 755-759.
- [6] Woodhead, I; Buchan, G; and Kulasiri D. 2001. Pseudo 3-D Moment Method for Rapid Calculation of Electric Field Distribution in a Low Loss Inhomogenous Dielectric. *IEEE Transactions on Antennas and Propagation*, 49:1117-1122
- [7] Woodhead, I. M; Riding, P; Christie, J. H; and Buchan, G D. 2003. Non-Invasive probing of the Near-Surface Soil Moisture Profile. *Fifth International Conference on Electromagnetic Wave Interaction with Water and Moist Substances*, Rotorua, NZ.
- [8] F. Kip, *Fundamentals of Electricity and Magnetism*, 2 ed., McGraw-Hill, 1962.
- [9] R. F. Harrington, *Field Computation by Moment Methods*, R E Kreiger, 1968.
- [10] S. Ramo, J. R. Whinnery, and T. Van Duzer, *Fields and Waves in Communication Electronics*, 3 ed., Wiley, New York, 1993.
- [11] J. H. Knight, P. A. Ferre, D. L. Rudolph, and R. G. Kachanowski, "A Numerical Analysis of the Effects of Coatings and Gaps Upon Relative Dielectric Permittivity Measurement with Time Domain Reflectometry," *Water Resour. Res.*, Vol. 33, 1997, pp. 1455-1460.
- [12] P. A. Ferre, D. L. Rudolph, and R. G. Kachanoski, "Spatial Averaging of Water Content by Time Domain Reflectometry: Implications for Twin Rod Probes with and without Dielectric Coatings," *Water Resour. Res.*, Vol. 32, 1996, pp. 271-279.
- [13] E. J. A. Spaans and J. M. Baker, "Simple Baluns in Parallel Probes for Time Domain Reflectometry," *Soil Sci. Soc. Am. J.*, Vol. 57, 1993, pp. 668-673.
- [14] Savitsky and M. J. E. Golay, "Smoothing and Differentiation of Data by Simplified Least Squares Procedures," *Analytical Chemistry*, Vol. 36, 1964, pp. 1627-1639.